Title
Magnetic vortex nucleation modes in static magnetic fields

Journal
AIP Advances, 7(10)

ISSN
2158-3226

Authors
Vaňatka, Marek
Urbánek, Michal
Jíra, Roman
et al.

Publication Date
2017-10-01

DOI
10.1063/1.5006235

Peer reviewed

Magnetic vortex nucleation modes in static magnetic fields

Marek Vaňatka[1,a], Michal Urbánek[1,2,b], Roman Jíra[2], Meena Dhankhar[1], Lukáš Flajšman[1], Mi-Young Im[3], Vojtěch Uhlíř[1], Jan Michalička[1] and Tomáš Šikola[1,2]

[1]*CEITEC BUT, Brno University of Technology, Technická 10, 616 00 Brno, Czech Republic*
[2]*Institute of Physical Engineering, Brno University of Technology, Technická 2, 616 69 Brno, Czech Republic*
[3]*Center for X-ray Optics, Lawrence Berkeley National Laboratory, Berkeley, California 94720, USA.*
Contact addresses: [a]marek.vanatka@ceitec.vutbr.cz, [b]urbanek@fme.vutbr.cz

The magnetic vortex nucleation process in micron-sized magnetic disks undergoes several phases with distinct spin configurations called the nucleation states. Before formation of the final vortex state, small submicron disks typically proceed through the so-called C-state while the larger micron-sized disks proceed through the more complicated vortex-pair state or the buckling state. This work classifies the nucleation states using micromagnetic simulations and provides evidence for their stability in static magnetic fields using magnetic imaging techniques and electrical transport measurements. Lorentz Transmission Electron Microscopy (LTEM) and Magnetic Transmission X-ray Microscopy (MTXM) are employed to reveal the details of spin configuration in each of the nucleation states, which are unambiguously identified using electrical probing by Anisotropic Magnetoresistance (AMR).

For all coauthors:

- Please check the author list for completeness and correctness including their affiliations
- Figures have got the sizes set according to the column width (1,3,4) and full page width (2) including the caption in this case. If you print them, it should be the final size
- Send me any comments in a copy of this word file, please use tracking changes.
- APL allows manuscripts up to 3500 words and figures are included… there is no room for adding much text

Magnetic vortices are flux-closing magnetization configurations known to occur in micro- or nano-size disks or polygons fabricated from soft magnetic materials like Permalloy. They consist of a magnetization curling in the disk plane and from a vortex core located at the center, where the magnetization points perpendicular to that plane[1–3]. A vortex state may be described by two independent parameters: the circulation, and polarity. Circulation is defined by the sense of magnetization curling (clockwise, $c=-1$ or counterclockwise, $c=1$) and the polarity is defined by the direction of the vortex core (pointing up, $p=1$ or down $p=-1$). The product cp defines the vortex handedness, either right-handed ($cp=1$) or left-handed ($cp=1$). The four distinct combinations of *c* and *p* in a single element promise possible applications related to multibit memory cells[4,5]. Other applications include logic circuits[6] or radio-frequency devices[7,8] using gyrotropic excitation of the vortex core with eigenfrequencies typically on the order of hundreds of MHz. Recent studies have shown magnetic vortices as spin wave emitters9 using two antiferromagnetically coupled disks in a heterostructure providing a system with high eigenfrequencies compared to a single magnetic disk with a vortex state.

Controlling the vortex states by switching the vortex polarity or circulation have been shown both in dynamic[10–14] and static[15–19] regimes. The circulation switching requires annihilation of the vortex by displacing the vortex core out of the magnetic disk, followed by nucleation of a new vortex in decreasing external field. The final state of the vortex depends on the exact course of the nucleation process, which received less attention in the literature than the vortex circulation and polarity switching. There are several works providing studies of the full magnetic vortex reversal with matched micromagnetic simulations[18,19] and few works about the vortex state formation in disks with broken symmetry arising from the Dzyaloshinskii–Moriya interaction[20] or the disk geometry[21]. Here we study the nucleation process of the magnetic vortex in slowly decreasing magnetic fields and show that three distinct nucleation pathways are possible, each proceeding through different spin configurations called nucleation states. The micromagnetic simulation of the three nucleation states are shown in Fig. 1. We used Object Oriented Micromagnetic Framework[22] (OOMMF) with the following parameters: a cell size of $4\times4\times4$ nm, saturation magnetization $M_s=800$ kA/m, exchange constant $A=13$ pJ/m. The first nucleation state, the *C-state*[15] is shown in Fig. 1(a). It consists of spins following the shape of the letter C in order to decrease the dipolar energy when compared to the disk in saturation. This state is common for rather small disks (approximately for diameters $D<400$ nm and thicknesses $t<20$ nm). Investigation of larger disks leads to two different and more complicated nucleation states: the vortex-pair state[23] and the buckling state[15,19,24] (Fig. 1(b) and Fig. 1(c) respectively].

The vortex-pair state is favored in larger disks with smaller thicknesses (D/t ratio ¿20), e.g. for $D=1$ μm the thickness t should be smaller than 50 nm. It consists of two vortex cores around which the magnetization is curling in the opposite sense keeping most of the spins pointing along the external field. Upon the field decrease, the cores move towards each other decreasing the net magnetization along the field direction until they annihilate and a single vortex core is formed in the disk. Micromagnetic simulations show that the two cores of the vortex-pair state have always opposite polarities and circulations of magnetization around them (giving the same handedness for both cores) providing the final vortex state to be fundamentally random for the symmetry reasons. However, in reality this cannot be assumed because the geometrical symmetry is always broken due to lithographic imperfections and surface roughness of the substrate.

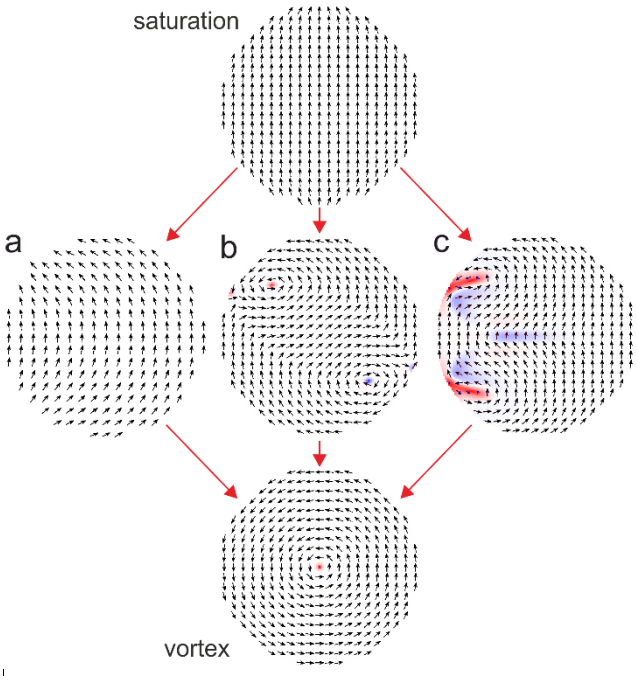

Fig. 1: Magnetic vortex nucleates upon the field decrease from saturation while undergoing one of the nucleation states visualized by micromagnetic simulations: **a** C-state, **b** vortex-pair state, **c** buckling state.

The buckling state is favored in disks with smaller D/t ratios $¿20$ (for example $D=1$ µm and $t=100$ nm. Although previously described and simulated[15,19,24], it has not been demonstrated experimentally. The characteristic feature of the buckling state are the three domain walls with m_z components and the in-plane magnetization curling around them as shown in Fig. 1(c). When the field is decreased, the three domain walls move towards each other until a vortex state is formed. The buckling state has lower symmetry than the vortex-pair state and the in-plane magnetization shape indicates the final circulation of the vortex – in case of Fig. 1c the circulation will be clockwise. Even though the situation is less evident for the final polarity state, the simulations show that the m_z domains at the disk edge will become dominant over the middle ones - in case of Fig. 1c the vortex core polarity will be defined by the m_z component of the red domains.

Experimental observation of the nucleation states by magnetic microscopies and anisotropic magnetoresistanc (AMR) involved Permalloy magnetic disks fabricated by electron beam lithography and the lift-off process. We used 30-nm and 200-nm thick SiN membranes as substrates for the Lorentz Transmission Electron Microscopy (LTEM) and the Magnetic Transmission X-ray Mcroscopy (MTXM), respectively. For the AMR measurements we used undoped Si (100) as a substrate and the disk fabrication was followed by a second lithography step in which a pair of Au contacts was fabricated in order to establish electrical connections to the disk.

The LTEM images (Fresnel mode) of the nucleation states are shown in the upper row of the Fig. 2. This method does not image the magnetization inside of the sample directly but it only reveals the domain wall structure as the images of neighboring domains shift against each other or apart from each other due to the Lorentz forces, thus creating positive or negative overlap yielding white or black contrast respectively. This disadvantage may be overcome by micromagnetic simulations of the corresponding magnetization states and then recalculating them into the LTEM contrast. For this purpose we used Micromagnetic Analysis to Lorentz TEM Simulation[25] (MALTS) to provide

comparison between the acquired images and the simulations. The images of LTEM contrast calculated by MALTS are in the second row of the Fig. 2 and the used magnetization distribution calculated by OOMMF in the third row of the Fig. 2. The external magnetic field needed for vortex annihilation and consequent gradual nucleation is applied by the TEM objective lens (which is normally turned off in the Lorentz mode). As this field is along the microscope optical axis, the sample was tilted by 30 degrees to gain an in-plane component of the magnetic field. The tilt also results in elliptical projections of the disks. LTEM images show a good agreement between the simulated and measured contrast for both the vortex-pair state [Fig. 32(a) and 2(b)] and the buckling state [Fig. 32(c) and 2(d)]. A reference vortex state at zero field is shown in Fig. 3e.

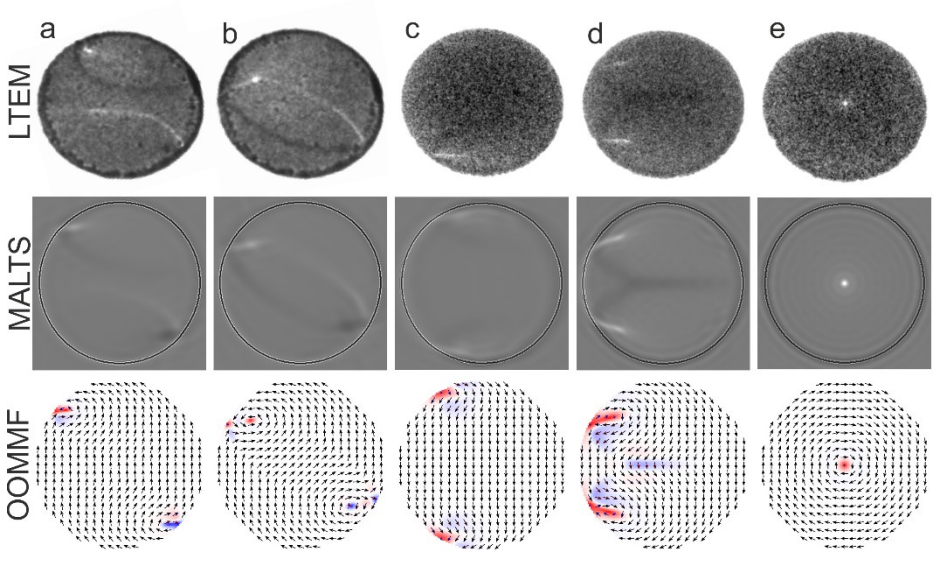

Fig. 2: Simulation and LTEM imaging of vortex nucleation states. Top row: LTEM observation; middle row: LTEM contrast simulated from the spin configurations shown in the bottom row: OOMMF micromagnetic simulations. Columns: **a**, **b** two consecutive configurations forming the vortex-pair state. **c**, **d** formation of the buckling state. **e** vortex state for reference.

The vortex-pair state nucleation process consists of two steps indicated in Fig. 32(a) and 2(b). The image in Fig. 32(a) is characterized by two black and white lines separating the three main in-plane domains containing in-plane magnetization in the disk. Additionally we can observe two spots where one of them is lighter and the other one darker than the rest of the contrast. This represents perpendicular domain walls featuring a larger magnetization curl (i.e. higher contrast). The two white and black lines move closer to each other upon decreasing the field until the perpendicular domain walls unpin from the disk boundary into two standalone vortex cores yielding the spin configuration of the vortex-pair state in Fig. 32(b). Further field decrease leads to the vortex nucleation. In case of the buckling state [Fig. 32(c) and 2(d)], the process is different. When the field decreases from saturation, the first step is the formation of perpendicular domain walls at the disk boundary yielding

light LTEM contrast in these positions. From this state, the buckling state is formed by moving the two domain walls towards each other, which is accompanied by gradual formation of a third perpendicular domain wall. The provided LTEM contrast then consists of a typical line passing through the disk center splitting towards the edge where the line bounces from the edge with reversed contrast [from black to white in case of Fig. 32(d)]. Further field decrease again introduces the vortex nucleation.

The nucleation process was also detected by measuring the associated resistance changes due to anisotropic magnetoresistance (AMR). Considering the experimental geometry presented in Fig. 3(a) and 3(b) with the magnetic field along the *y*-axis, the highest resistance is measured at saturation where the spins are aligned along both the field and the current density j. Then each of the states comes with a lower level of electrical resistance following the AMR law for resistivity: $\rho(\varphi)=\rho_{\perp}+(\rho_{\parallel}-\rho_{\perp})\cos^2\varphi$, where φ is the angle between the vector of current density j and the vector of magnetization m. The OOMMF vector maps were used to calculate the resistance of each state along the hysteresis loop in order to predict the shape and specific features for the nucleation processes going through the vortex-pair state or the buckling state. The calculation consisted of assigning the resistance value to each simulation cell by following the AMR formula and then connecting all cells together to a resistor network and combining their resistances. The two constants $\rho_{\perp}$ and $\rho_{\parallel}$ were measured in another experiment for Permalloy layers to be $\rho_{\perp}=7.40\cdot10^{-7}\,\Omega\,\mathrm{m}$ and $\rho_{\parallel}=7.50\cdot10^{-7}\,\Omega\,\mathrm{m}$.

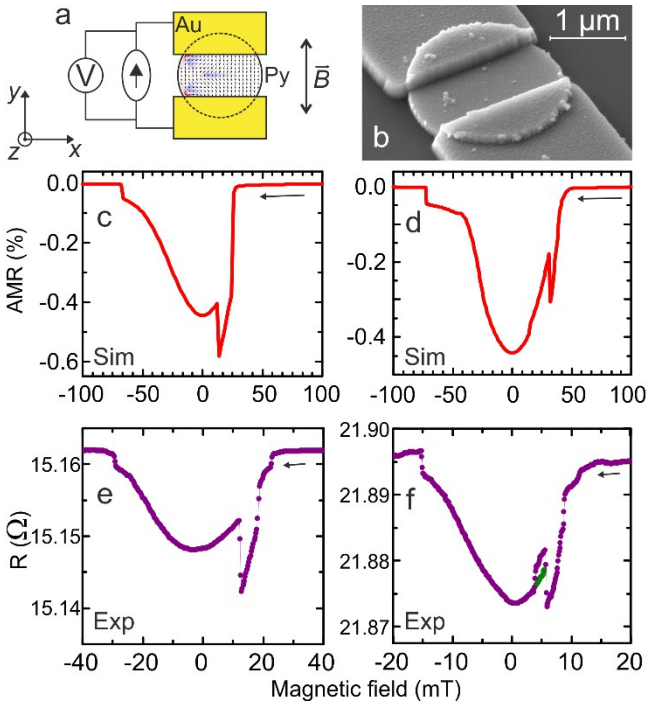

Fig. 3: Modeling and measurement of AMR probing the vortex nucleation mechanism. a) schematics of the sample geometry with the electrical connection. b) SEM micrograph of the Permalloy disk detail and Au contacts prepared in a two-step lithography process. c), e) simulation and experimental data, respectively, of the AMR upon the vortex nucleation via the vortex-pair state and d), f) the buckling state. The magnetic field is swept from positive to negative values.

Fig. 3(c) and Fig. 3(e) show the simulated and experimental AMR spectra for the magnetic field sweep in the direction from positive to negative field with vortex nucleation going through the

vortex-pair state. The simulated spectrum in Fig. 3(c) shows an abrupt drop of resistance at 24 mT where the vortex-pair state is formed in the disk and then the resistance decreases linearly upon lowering the field. This is associated with the motion of the two cores of the vortex-pair state towards each other until the two cores annihilate into a single vortex state at 12 mT, which leads to an abrupt increase of the resistance. The following step represents the reversible displacement of the vortex core in magnetic field. After reversing the field orientation, the annihilation takes place at -68 mT where the resistance jumps up to the saturation level. The experimental spectrum in Fig. 3(e) shows the same features as those predicted by the model. The only difference is the nucleation part, where the resistance is lowering in several steps due to pinning of magnetization, which delays the formation of the vortex-pair state. The experimental values of the nucleation and annihilation fields are lower than the simulated values as the simulations are performed at zero temperature.

The AMR spectra in Fig. 3(d) and Fig. 3(f) show similar general behavior compared to the spectra in Figs. Fig. 3(d) and Fig. 3(e) but few significant differences associating them to the buckling state nucleation process. There is a similar decrease in resistance connected with the nucleation process but the resistance decreases gradually all the way from saturation (without the abrupt drop from saturation) and the depth of the resistance dip before the nucleation is shallower when compared to the vortex-pair state. The nucleation occurs at 32 mT where the resistance suddenly increases. A significant point of interest is at 15 mT where a small drop in resistance is present. When inspecting the simulated states at each point around this drop, it was found that the nucleated vortex state does not have a single vortex core but instead has two vortex cores with an antivortex in between them, called the vortex-antivortex-vortex triplet (VAV triplet, see detail in Fig. 4: Detail of the VAV triplet nucleated from the buckling state. MTXM images (top row) with contrast are compared to the OOMMF simulations (bottom row).). This VAV triplet is stable in a range of a few mT. After further field decrease it annihilates into a single vortex core resulting in a small drop in the AMR spectrum. This state was electrically detected with its feature shown in the purple curve of Fig. 3(f) between 4-6 mT. However, when the measurement was repeated multiple times, this drop was present only in about 30% of all field sweeps while during the other sweeps we measured the green trace in Fig. 3(f). This is attributed to lower stability of the VAV triplet when compared to the vortex state with a single core at the same magnetic field. The VAV triplet was further investigated using Magnetic Transmission X-ray spectroscopy (MTXM) carried out at beamline 6.1.2 at the Advanced Light Source (ALS) in Berkeley, California. Images with a spatial resolution of 25 nm were recorded using x-ray magnetic circular dichroism (XMCD) as magnetic contrast for a fixed circular polarization of the x-ray beam at the Fe L3 edge (707 eV). The VAV triplet was nucleated from the buckling state as predicted by the simulation (Fig. 4: Detail of the VAV triplet nucleated from the buckling state. MTXM images (top row) with contrast are compared to the OOMMF simulations (bottom row).). The two bottom images show the corresponding simulated images with the gray scale matched to the m_z component. The detail on the right side shows a close-up of the magnetization distribution in the VAV triplet.

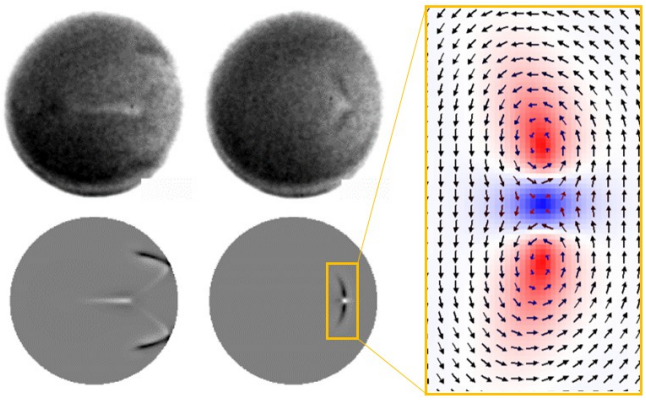

Fig. 4: Detail of the VAV triplet nucleated from the buckling state. MTXM images (top row) with m_z contrast are compared to the OOMMF simulations (bottom row). A simulated image of the VAV triplet is shown in the close-up.In conclusion, we studied the nucleation process of magnetic vortices in Permalloy disks in slowly changing magnetic fields. Two different nucleation states, the vortex-pair state and the buckling state, were verified by LTEM imaging with a good agreement to the simulated contrast by MALTS. The existence of stable vortex-antivortex-vortex triplet was confirmed by MTXM. We have also shown that all important spin structures occurring during the nucleation may be detected electrically by using the AMR phenomena. Results of this work could provide a route for further application in the field of magnonics where the stabilization of more complicated states (by a biasing field) than the simple vortex state would be the basis for their further RF excitation introduced either by exciting waveguide or spin torque current. It was analyzed in simulation that especially the VAV triplet, being a highly confined spin structure, has eigenfrequencies in order of 10^8 Hz suitable for spin wave generation in a single magnetic element allowing for a parallel approach to the already presented work using antiferromagnetically coupled vortices as spin wave emitters[9].

References:

[1] A. Hubert and R. Schäfer, *Magnetic Domains - The Analysis of Magnetic Microstructures* (Springer, 1998).

[2] R.P. Cowburn, D.K. Koltsov, A.O. Adeyeye, M.E. Welland, and D.M. Tricker, Phys. Rev. Lett. **83**, 1042 (1999).

[3] T. Shinjo, Science (80-.). **289**, 930 (2000).

[4] S. Bohlens, B. Krüger, A. Drews, M. Bolte, G. Meier, and D. Pfannkuche, Appl. Phys. Lett. **93**, 142508 (2008).

[5] S.-K. Kim, K.-S. Lee, Y.-S. Yu, and Y.-S. Choi, Appl. Phys. Lett. **92**, 22509 (2008).

[6] H. Jung, Y.S. Choi, K.S. Lee, D.S. Han, Y.S. Yu, M.Y. Im, P. Fischer, and S.K. Kim, ACS Nano **6**, 3712 (2012).

[7] V. Novosad, F. Fradin, P. Roy, K. Buchanan, K. Guslienko, and S. Bader, Phys. Rev. B **72**, 24455 (2005).

[8] N. Hasegawa, S. Sugimoto, H. Fujimori, K. Kondou, Y. Niimi, and Y. Otani, Appl. Phys. Express **8**, 63005 (2015).

[9] S. Wintz, V. Tiberkevich, M. Weigand, J. Raabe, J. Lindner, A. Erbe, A. Slavin, and J. Fassbender, Nat. Nanotechnol. **11**, 948 (2016).

[10] B. Van Waeyenberge, A. Puzic, H. Stoll, K.W. Chou, T. Tyliszczak, R. Hertel, M. Fähnle, H. Brückl, K. Rott, G. Reiss, I. Neudecker, D. Weiss, C.H. Back, and G. Schütz, Nature **444**, 461 (2006).

[11] M. Kammerer, M. Weigand, M. Curcic, M. Noske, M. Sproll, A. Vansteenkiste, B. Van Waeyenberge, H. Stoll, G. Woltersdorf, C.H. Back, and G. Schuetz, Nat. Commun. **2**, 279 (2011).

[12] R. Hertel, S. Gliga, M. Fähnle, and C. Schneider, Phys. Rev. Lett. **98**, 117201 (2007).

[13] V. Uhlíř, M. Urbánek, L. Hladík, J. Spousta, M.-Y. Im, P. Fischer, N. Eibagi, J.J. Kan, E.E. Fullerton, and T. Šikola, Nat. Nanotechnol. **8**, 341 (2013).

[14] M. Urbánek, V. Uhlíř, C.-H. Lambert, J.J. Kan, N. Eibagi, M. Vaňatka, L. Flajšman, R. Kalousek, M.-Y. Im, P. Fischer, T. Šikola, and E.E. Fullerton, Phys. Rev. B **91**, 1 (2015).

[15] K. Guslienko, V. Novosad, Y. Otani, H. Shima, and K. Fukamichi, Phys. Rev. B **65**, 1 (2001).

[16] K.Y. Guslienko, V. Novosad, Y. Otani, H. Shima, and K. Fukamichi, Appl. Phys. Lett. **78**, 3848 (2001).

[17] V. Novosad, K.Y. Guslienko, H. Shima, Y. Otani, K. Fukamichi, N. Kikuchi, O. Kitakami, and Y. Shimada, IEEE Trans. Magn. **37**, 2088 (2001).

[18] M. Rahm, M. Schneider, J. Biberger, R. Pulwey, J. Zweck, D. Weiss, and V. Umansky, Appl. Phys. Lett. **82**, 4110 (2003).

[19] S.R. Bakaul, B.L. Wu, G.C. Han, and Y.H. Wu, Appl. Phys. Lett. **97**, 1 (2010).

[20] M.-Y. Im, P. Fischer, K. Yamada, T. Sato, S. Kasai, Y. Nakatani, and T. Ono, Nat. Commun. **3**, 983 (2012).

[21] M.-Y. Im, K.-S. Lee, A. Vogel, J.-I. Hong, G. Meier, and P. Fischer, Nat. Commun. **5**, 5620 (2014).

[22] M.J. Donahue and D.G. Porter, Interag. Rep. NISTIR 6376 (National Inst. Stand. Technol. Gaithersburg, MD, 1999) (n.d.).

[23] K.S. Buchanan, P.E. Roy, M. Grimsditch, F.Y. Fradin, K.Y. Guslienko, S.D. Bader, and V. Novosad, Nat. Phys. **1**, 172 (2005).

[24] T. Wren and O. Kazakova, J. Appl. Phys. **117**, 17E134 (2015).

[25] S.K. Walton, K. Zeissler, W.R. Branford, and S. Felton, IEEE Trans. Magn. **49**, 4795 (2013).

[26] P. Fischer, Mater. Today **13**, 14 (2010).